Available online at www.sciencedirect.com
SCIENCE DIRECT
Journal of Catalysis 230 (2005) 214–225
JOURNAL OF CATALYSIS
www.elsevier.com/locate/jcat

Interaction between sulfated zirconia and alkanes: prerequisites for active sites—formation and stability of reaction intermediates

Xuebing Li, Katsutoshi Nagaoka, Laurent J. Simon, Johannes A. Lercher

Technische Universität München, Department of Chemistry, Lichtenbergstraße 4, 85747 Garching, Germany

Sabine Wrabetz, Friederike C. Jentoft

Department of Inorganic Chemistry, Fritz-Haber-Institut der Max-Planck Gesellschaft, Faradayweg 4-6, 14195 Berlin, Germany

Cornelia Breitkopf, Silke Matysik, Helmut Papp *

Universität Leipzig, Institute of Technical Chemistry, Linnéstr. 3, 04103 Leipzig, Germany

Received 22 September 2004; revised 24 November 2004; accepted 26 November 2004

Available online 13 January 2005

Abstract

Two sulfated zirconia catalysts were prepared via sulfation and calcination of zirconium hydroxide at 873 K; the zirconium hydroxide had been aged at room temperature for 1 h (SZ-1) or aged at 373 K for 24 h (SZ-2). SZ-1 was active for *n*-butane isomerization at 373 K; SZ-2 reached a similar performance level only at 473 K. Both materials contained about 9 wt% sulfate and were tetragonal. Because of a lower BET surface area (105 vs. 148 m^2/g) SZ-1 featured a higher sulfate density, and XRD and EXAFS analysis showed larger (ca. 10 nm) and more well ordered crystals than for SZ-2. *n*-Butane TPD on SZ-1 showed a butene desorption peak at low temperature, whereas no obvious butene desorption was observed with SZ-2, suggesting that SZ-1 has a higher oxidizing power at low temperature than SZ-2. The number of sites capable of dehydrogenation are less than 5 μmol/g, because the differential heats of *n*-butane adsorption as measured by microcalorimetry were 45–60 kJ/mol for higher coverages, indicating weak and reversible interaction. TAP experiments describe the adsorption and desorption behavior of *n*-butane at different activity states and are the basis for a simple adsorption model. Reactant pulses and purge experiments show that the active species, presumably formed in an oxidative dehydrogenation step, are stable at the surface under reaction conditions.

Keywords: Sulfated zirconia; Alkanes; Isomerization; Active sites; Reaction intermediates; Transient measurements

1. Introduction

Sulfated zirconia, capable of converting alkanes to their isomers at low temperatures, attracted significant interest in recent years [1–4]. Even though numerous investigations focused on the preparation of sulfated zirconia, the essential procedure is still unclear, since many factors significantly affect the resultant sulfated zirconia, such as the precursor for sulfation [5–7], the sulfation agent [8,9], or the calcination conditions [10–14].

It was claimed that an active sulfated zirconia can only be prepared from amorphous zirconia hydroxide [15], obtained from hydrolysis of zirconium salts, that is, $ZrOCl_2$, $ZrCl_4$, or $ZrO(NO_3)_2$. Sulfation of crystalline zirconia was claimed to result in inactive sulfated zirconia. Recently, however, the preparation of active sulfated zirconia by sulfation of crystalline zirconia has also been reported [16,17]. The calcination of sulfated amorphous zirconium hydroxide in the temperature range 723–923 K always yielded predominantly the metastable tetragonal zirconia phase, which was

* Corresponding author.
E-mail address: papp@sonne.tachemie.uni-leipzig.de (H. Papp).

0021-9517/$ – see front matter
doi:10.1016/j.jcat.2004.11.045

believed to be the catalytically active phase [18–20]. In spite of this, monoclinic sulfated zirconia was also recently shown to be active for *n*−butane isomerization [21,22], but the activity was lower than that of tetragonal zirconia.

When Arata et al. [2,14] discovered the property of sulfated zirconia for butane isomerization at room temperature, it was categorized as a superacid, since only superacids are claimed to activate light alkanes at such a temperature. However, experiments using NMR [23,24], UV–vis [25], or IR spectroscopy [26,27] revealed that the acidity of sulfated zirconia is not higher than that of sulfuric acid. Alternatively, alkane isomerization may be related to the generation of olefins via oxidative processes [28–30]. In this context it should be mentioned that several papers have demonstrated the promoting effect of butenes for *n*-butane isomerization, via formation of carbenium ions on the catalyst surface [31–33].

In general, *n*-butane skeletal isomerization on sulfated zirconia or other sulfated metal oxide shows an induction period at low temperature, which is assumed to be due to the formation of the active species [34]. After the activity reaches its maximum, the catalyst deactivates, while coke is being formed on the surface [35]. The rate constant of deactivation decreased dramatically when alkenes in the feed were eliminated via a suitable trap [36,37].

Here we use two sulfated zirconia materials of very different activities, but both tetragonal and equal in sulfate content, to discriminate on a finer scale between relevant and irrelevant properties. In addition to extensive structural and site characterization, we investigate the capacity of the materials to generate butenes and the dynamics of the catalytic behavior with variations in reaction temperature and feed composition on a minute to hour scale.

2. Experimental

2.1. Catalyst preparation

Zirconium hydroxide powders were prepared by precipitation of $ZrO(NO_3)_2$ with NH_4OH in water at pH 8.4 with stirring. The resulting precipitate was aged in solution at room temperature for 1 h followed by filtering, washing, and drying at 373–393 K, denoted as Z-1. Alternatively, the precipitate was aged at 373 K for 24 h and processed as above; this sample is denoted Z-2. We obtained sulfated zirconias (SZ-1 and SZ-2) by sulfating the powders prepared above (Z-1 and Z-2) with $(NH_4)_2SO_4$ (20 mol%) followed by calcination at 873 K for 3 h in flowing air.

2.2. Catalyst characterization

The sulfate contents (SO_4^{2-} wt%) of the catalysts were determined by ion chromatography (IC) as described in the literature [38]. For this, 0.02 g of sulfated zirconia was suspended in a 0.1 N solution of NaOH, and the solution was filtered with a 0.45-μm filter. The sulfate content was measured by ion chromatography (Metrohm; 690 ion chromatograph equipped with an IC anion column). The BET surface area of sulfated zirconia was determined with a PMI automated BET-sorptometer at 77.3 K with nitrogen as the analysis gas. X-ray diffractometry (XRD) of the catalysts was performed in transmission geometry on a STOE STADI-P X-ray diffractometer equipped with a primary monochromator and a curved position-sensitive detector with an internal resolution of 0.01°, with Cu-K_α radiation ($\lambda = 1.542$ Å). Samples were mixed 1:1 with corundum, which was used as an internal standard. Nonsulfated samples were analyzed with a Philips X'Pert-1, also with Cu-K_α radiation. Scanning electron microscopy (SEM) was conducted on a Hitachi S-4000 microscope equipped with a cold field emission gun at an acceleration voltage of 5 kV. X-ray absorption spectra of the Zr *K*-edge (17.998 keV) were recorded at beamline X1 at the Hamburger Synchrotron Radiation Laboratory (HASYLAB) with a Si(311) double crystal monochromator. The storage ring was operated at 4.45 GeV with injection currents of 150 mA. X-ray absorption fine structure (XAFS) analysis was performed with the software package WinXAS v2 [39].

To estimate the concentration of Brønsted and Lewis acid sites, IR spectra for pyridine adsorption tests were obtained at 373 K in vacuum with a Perkin–Elmer 2000 spectrophotometer at 4 cm^{-1} resolution. Samples were pressed into wafers, heated to 673 K at 10 K/min, kept at 673 K for 2 h (residual pressure of 10^{-6} hPa), and exposed to pyridine (0.1 hPa) at 373 K for 60 min, followed by evacuation at this temperature for 30 min. The number of sites available for alkane adsorption was determined from measurement of adsorption isotherms of propane, *n*-butane, and isobutane (all Messer–Griesheim, 99.5%) at 313 K after outgassing at 723 K in vacuum. The differential heats of adsorption were determined with a SETARAM MS-70 Calvet calorimeter. The setup is described in detail in [40]. The error bars given for the data result from the uncertainty in the heat generated by valve opening, which contributes to the heat signal for each dosing step.

2.3. Temperature-programmed desorption of *n*-butane

The temperature-programmed desorption of *n*-butane was performed with a vacuum system. The sulfated zirconia sample was activated under vacuum at 673 K for 2 h and cooled to 323 K for *n*-butane adsorption. *n*-Butane (2 hPa) (Messer–Griesheim; 99.5%, purified with a H-Y zeolite trap for alkene removal) was allowed to equilibrate with the sample for 5 min. The sample was heated to 873 K at 10 K/min. The desorbing species were analyzed with a mass spectrometer (QME 200, Pfeiffer vacuum).

2.4. Isomerization of *n*-butane

n-Butane isomerization was carried out in a quartz microtube reactor (8 mm i.d.) under atmospheric pressure. Sul-

fated zirconia pellets (0.2 g, 315–710 μm) were loaded into the reactor and activated in situ at 673 K for 2 h in flowing He (10 ml/min). The catalyst was cooled to the desired reaction temperature, and the reactant mixture (5% *n*-butane in He, total flow of 20 ml/min) was passed through the catalyst bed. We purified *n*-butane (Messer–Griesheim; 99.5%) of alkene impurities by flushing it through a trap containing H-Y zeolite. Alkenes were not detected in the reactant mixture after purification. The reaction products were analyzed with an on-line HP 5890 gas chromatograph (GC) equipped with a capillary column (Plot Al_2O_3, 50 m × 0.32 mm × 0.52 mm) connected to a flame ionization detector (FID). The rate of isobutane formation was taken as a measure of catalytic activity.

The influence of temperature on the catalytic behavior of both catalysts was studied. After reaction at 373 K over 60 h, when SZ-1 was deactivated completely and SZ-2 had not shown any activity, 20 ml/min of He flow was passed through the catalyst bed for 30 min. The reaction was then restarted after the temperature had been increased to 473 K.

Pulsing during the induction period of the reaction on SZ-1 at 373 K was performed by alternately changing the reactant (5% *n*-butane) and He flow every minute. A stop-restart experiment was conducted on the SZ-1 catalyst at 373 K during the deactivation phase. At the end of the induction period, the catalyst bed was purged with He for a certain time, and then the reaction was restarted. This procedure was repeated several times.

2.5. Temporal analysis of products switch experiments with *n*-butane

We probed surface sites and their reactivity in a TAP-II reactor [41] by pulsing *n*-butane over the fresh catalysts and over catalysts that had been used in isomerization in a flow experiment at 423 K. Pulse responses were analyzed with a quadrupole mass spectrometer (QMS) from HIDEN, where single masses (m/e) of interest can be followed. The reactor was filled with a corundum/catalyst mixture analogous to one used in atmospheric flow experiments. For SZ-1, 300 mg of catalyst was mixed with 700 mg of corundum, whereas for SZ-2, which is more voluminous, 258 mg of catalyst material was mixed with 604 mg of corundum. The particle diameter for all materials was 0.1–0.315 mm. The temperature was controlled by a thermocouple positioned in the center of the bed.

Neon was used as the reference gas. Knudsen diffusion in the reactor during pulse experiments was ensured by control of the pulse intensity of the pulses. The shape of the response curves has to be independent from the pulse size. Pulse sizes were then kept constant. Reactant mixtures were used at a constant pulse width of 130 μs and mixed in the blending tank with 200 hPa inert gas and 200 hPa reactant gas. A single experiment consisted of several cycles of pulsing with signal averaging (in general 10 pulses; for m/e of lower intensity up to 50) to improve the signal-to-noise ratio.

Samples were activated before use in TAP at 573 K for 2 h in vacuum in the microreactor and then cooled down at 10 K/min to the reaction temperature. The fresh samples were exposed to single pulses of *n*-butane (Messer–Griesheim; 99.5%) first. We conducted the flow experiments by closing the slide valve of the TAP reactor and exposing the microreactor to a constant flow of 2 ml *n*-butane (Messer–Griesheim; 99.95%) in 18 ml helium. The reaction products were analyzed by on-line GC (Shimadzu).

n-Butane was monitored for all possible fragments known for C_4 alkanes. Only their main mass fragments ($m/e = 27$, 29, 41, 43, 58) and their ratios are discussed in detail here.

Modeling of a simple first-order adsorption rate constant was performed with modeling software by Schuurman and Gleaves [41], which assumes a first-order Langmuir adsorption for the reactant in a one-zone model.

3. Results

3.1. Catalyst characterization

BET surface areas, pore sizes, particle sizes, sulfate contents, and acid concentrations of different samples are compiled in Table 1. The zirconium hydroxide samples without thermal treatment exhibited the highest BET surface areas: uncalcined Z-1, 288 m^2/g; uncalcined Z-2, 342 m^2/g. Calcination at 873 K for 3 h converted zirconium hydroxide to zirconia and caused a significant BET surface area decrease: calcined Z-1, 49 m^2/g; calcined Z-2, 76 m^2/g. Calcination at 873 K for 3 h of zirconium hydroxide doped with sulfate also resulted in a loss of BET surface area. However, the calcined sulfate-doped samples had higher BET surface areas than the calcined undoped samples: SZ-1, 105 m^2/g; SZ-2, 148 m^2/g (twice that of calcined Z-1 and Z-2, respectively). The pore and particle size distributions of the calcined samples indicate that the calcined sulfate-doped and undoped zirconia samples were all mesoporous materials with irregular pores. The difference in the morphologies of SZ-1 and SZ-2 becomes evident from scanning electron microscopy (see Fig. 1). The SZ-1 particles were typically 5–20 μm in size; the surfaces exhibit smooth and stepped regions, and often smaller particles were found to be adhering. SZ-2 consisted predominantly of particles 1–5 μm in diameter, which occasionally enveloped larger particles.

Fig. 2a shows the XRD patterns for SZ-1, SZ-2, Z-1, and Z-2, which were all calcined at 873 K for 3 h in air. The calcined Z-1 was monoclinic and calcined Z-2 was tetragonal, which indicates that Z-1 was more sensitive to the thermal treatment than Z-2. Both calcined sulfated materials exhibited only reflections of the tetragonal phase. Normalization to internal standard corundum demonstrates that the reflections of SZ-2 are lower in intensity and broader than those of SZ-1 (Fig. 2b). The sizes of the crystalline domains as obtained via the Scherrer equation were 9.9 nm for SZ-1 and 7.5 nm for SZ-2.

Table 1
Preparation and properties of raw materials

	Z-1 uncalcined	SZ-1 uncalcined	Z-2 uncalcined	SZ-2 uncalcined
Precursor	Precipitation from $ZrO(NO_3)_2$ with NH_4OH until pH 8.4			
Aging	1 h at room temperature		24 h at 373 K	
Drying	After filtering and washing dried at 373–393 K			
Sulfation	–	$(NH_4)_2SO_4$ 20 mol%	–	$(NH_4)_2SO_4$ 20 mol%
SO_4^{2-} (wt%)	–	13.4	–	n.d.
BET surface area (m^2/g)	288	n.d.	342	n.d.
	Z-1 calcined	SZ-1 calcined	Z-2 calcined	SZ-2 calcined
Calcination	Flowing air, 873 K, 3 h			
BET surface area (m^2/g)	49	105	76	148
Pore size (nm)	8.0	3.5	7.0	3.7
Crystallite size (nm)	12.6	9.9	11.0	7.5
SO_4^{2-} (wt%)	–	9.0	–	8.9
SO_4^{2-} H_2O leached (wt%)	–	2.5	–	3.0
Brønsted acid sites				
(mmol/g)	n.d.	0.069	n.d.	0.047
(μmol/m^2)		0.66		0.32
n-Butane adsorption				
(mmol/g) at 1 kPa	n.d.	0.062	n.d.	0.056
(μmol/m^2) at 1 kPa		0.51		0.38

n.d.: not determined.

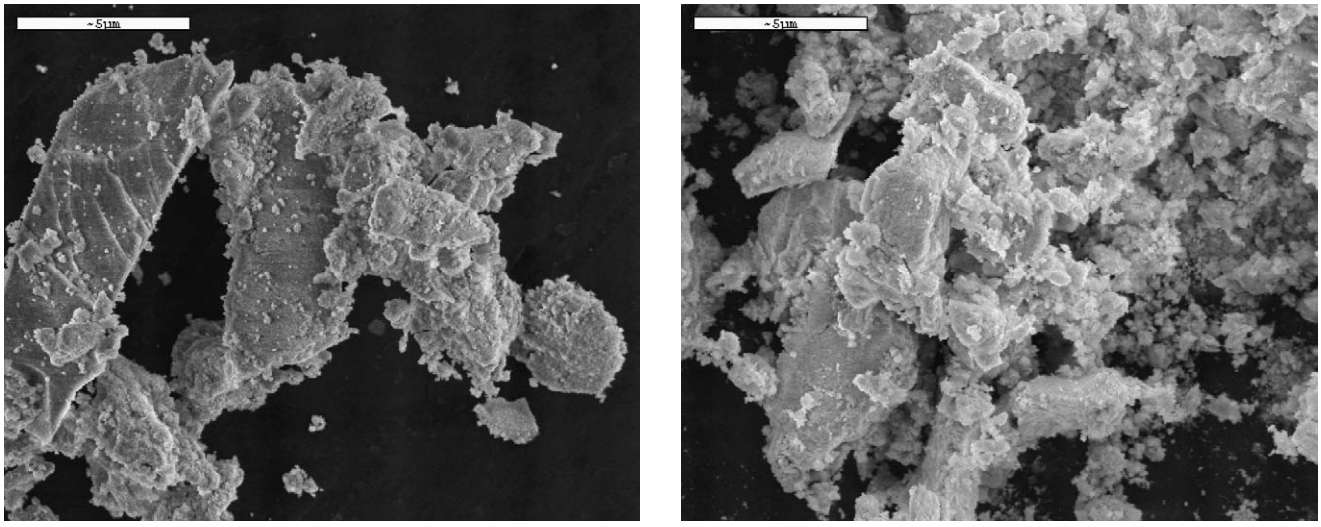

(a) (b)

Fig. 1. SEM images of (a) SZ-1 and (b) SZ-2.

These findings are corroborated by Zr K edge XAFS (see Fig. 3). The radial distribution functions, consistent with tetragonal or cubic zirconia, showed a lower intensity in the second and higher maxima for SZ-2 than for SZ-1. These higher shells are dominated by Zr–Zr contributions, and the decreased intensity may indicate a reduction in the Zr–Zr coordination due to smaller crystal domains. In addition, the reduced intensity may indicate an increase in the disorder of the structure, caused by strain, a small amount of a less ordered crystalline, or amorphous ZrO_2 phase.

3.2. Surface sites

The sulfate content of the uncalcined SZ-1 was 13.4%, whereas calcination at 873 K for 3 h in air resulted in a sulfate content of 9.0 wt%, which indicates that the high-temperature treatment eliminated approximately 30% of the sulfate groups. The sulfate contents of the resulting two calcined sulfated zirconia samples, SZ-1 and SZ-2, were both 9% in SO_4^{2-} wt%. This is higher than a hypothetical monolayer, if 0.31 nm^2 is assumed to be the surface area occupied

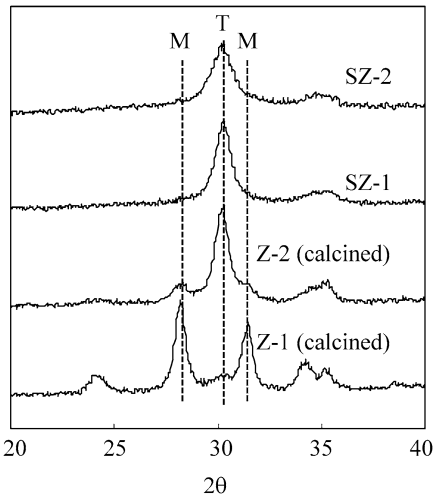

(a)

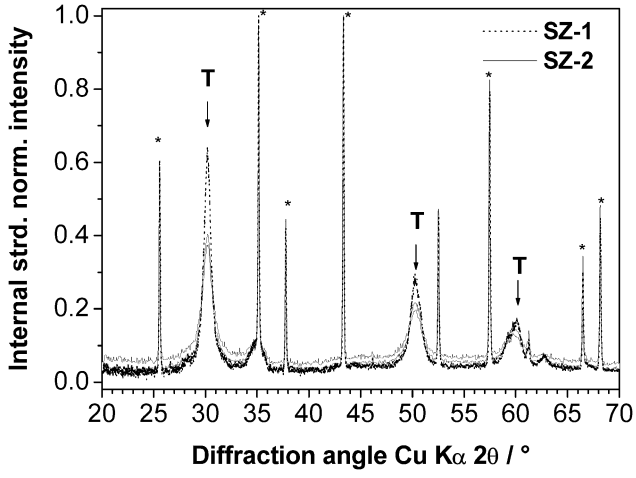

(b)

Fig. 2. XRD patterns of (a) calcined Z-1, Z-2, SZ-1, and SZ-2 and (b) calcined SZ-1 and SZ-2 measured with internal standard. M, monoclinic phase; T, tetragonal phase; *, internal standard corundum.

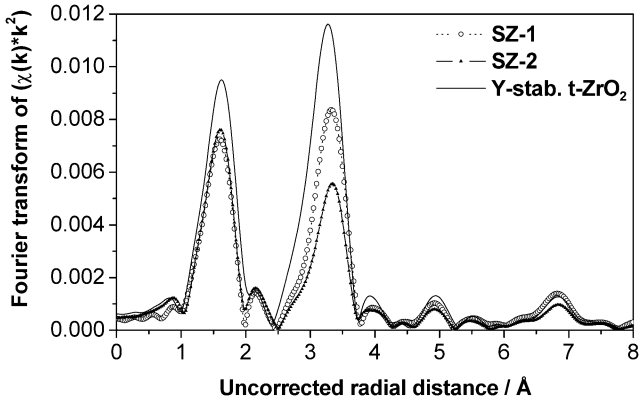

Fig. 3. Uncorrected radial distribution function for Zr K-edge of SZ-1, SZ-2, and an yttria-stabilized reference material.

by a SO_4^{2-} group based on its kinetic diameter [42]. The water-soluble sulfate fractions were 2.5 and 3.0 wt% for SZ-1 and SZ-2, respectively.

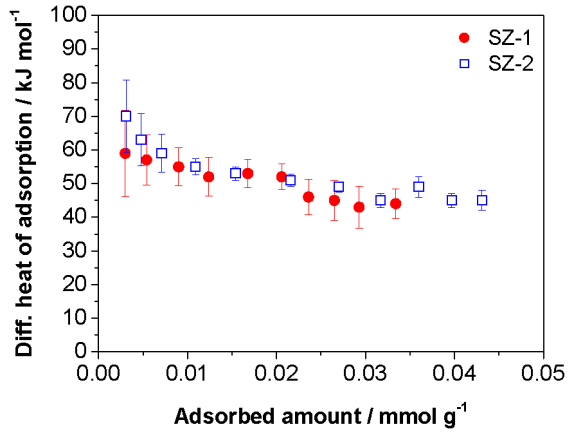

Fig. 4. Differential heats of adsorption of n-butane on SZ-1 and SZ-2 as a function of coverage. Activation at 723 K in vacuum, adsorption at 313 K.

The Brønsted acid site concentration (determined by adsorption of pyridine) of calcined SZ-1 was 0.069 mmol/g, which is higher than the 0.047 mmol/g observed with calcined SZ-2. Thus, SZ-1 provides 1.5 times as many Brønsted sites as SZ-2. This ratio was also confirmed by impedance spectroscopy, with which the relative concentrations of protonated pyridine molecules were also explored [43].

Alkane sorption sites on both materials were probed by adsorption of propane and butanes. Adsorption isotherms could be adequately described by a first-order Langmuir model for low pressures. The curvature at higher pressures could be reproduced with a higher order Langmuir model, but a slightly better fit was obtained with a Freundlich model. The differential heats decline with coverage, which is considered in the Freundlich model, but the decline is very gentle, so that the Langmuir model, which assumes uniform heats, is still a reasonable match. The Freundlich isotherms were used to estimate the number of sites covered at the typical alkane partial pressure of 5 kPa. Typical C_4 coverages at 5 kPa were between 85 and 160 μmol g^{-1}. The difference in the concentration of sites between the two catalysts, however, was not larger than differences arising through variation of the activation temperature. The heats of adsorption decreased slightly with coverage. For all three alkanes on both catalysts, differential heats of about 60 kJ mol^{-1} were determined at a coverage of ca. 5 μmol g^{-1}. The heats slowly declined to about 45 kJ mol^{-1} at a coverage of 30 μmol g^{-1}. The presence of a small amount of sites (i.e., < 5 μmol g^{-1}) with a different heat of adsorption cannot be excluded; however, data scatter considerably at coverages below 2–5 μmol g^{-1}. For the majority of sites, there were no significant differences between SZ-1 and SZ-2 in the differential heats (see, for example, n-butane adsorption, Fig. 4).

3.3. n-Butane temperature-programmed desorption

Figs. 5a and b shows the TPD after n-butane was adsorbed at 323 K on sulfated zirconia samples SZ-1 and SZ-2. Butene ($m/e = 56$) was the most abundant desorbing

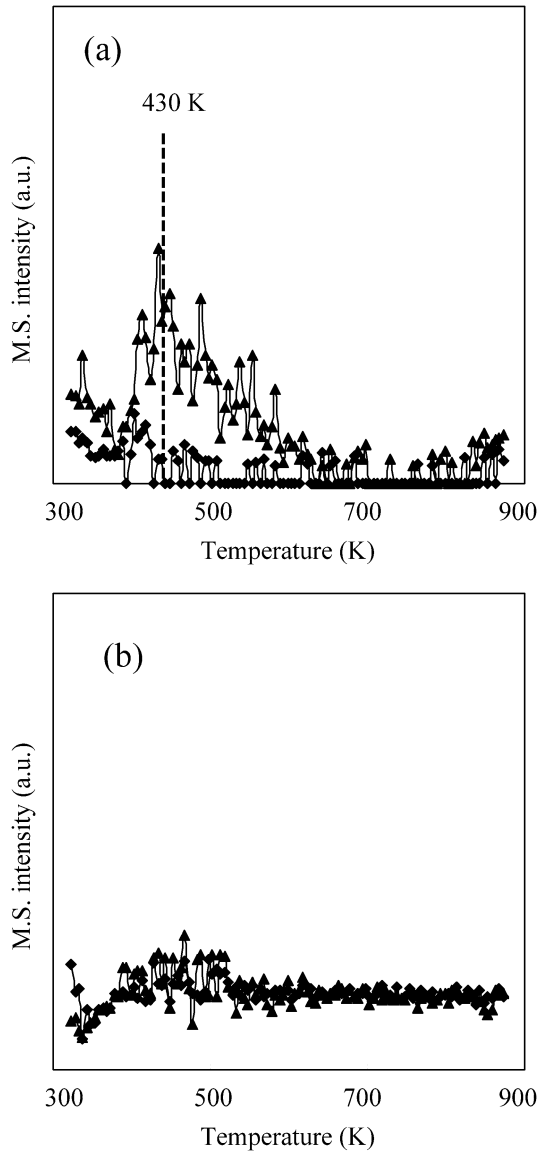

Fig. 5. n-Butane TPD profiles (a) SZ-1 and (b) SZ-2, (▲) butene ($m/e = 56$), (◆) butane ($m/e = 58$).

species, with an intense peak at 430 K on SZ-1. However, no obvious butene desorption peak was observed in n-butane TPD on SZ-2 at this temperature. Much lower intensities of butene and butane were observed in the gas phase up to 700 K for both catalysts, SZ-1 and SZ-2.

3.4. Catalytic experiments at atmospheric pressure

3.4.1. Activity of n-butane isomerization on SZ-1 and SZ-2

Fig. 6 shows the n-butane isomerization activity versus time on stream (TOS) of SZ-1 and SZ-2 at 373 K. SZ-1 showed a much higher catalytic activity than SZ-2, which was almost inactive at 373 K under the conditions used. An induction period characterized by a steady increase in the catalytic activity was observed during n-butane reaction on SZ-1, followed by deactivation. The maximum conversion for SZ-1 at 373 K was 0.9%. The product of n-butane reaction is primarily isobutane with 95–96% selectivity. The main by-products are propane and pentanes (n-pentane and iso-pentane with a ratio of 1:4).

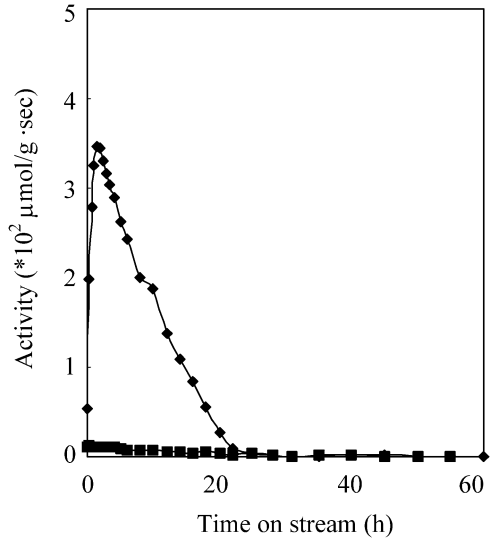

Fig. 6. n-Butane reaction rate versus time on stream at 373 K on (◆) SZ-1 and (■) SZ-2.

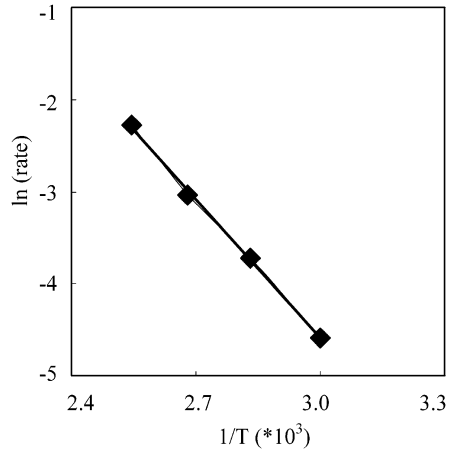

Fig. 7. Arrhenius profile of n-butane isomerization on SZ-1 at temperature range of 333–393 K.

Fig. 7 shows the Arrhenius correlation of n-butane isomerization on SZ-1 at the reaction temperature from 333 to 393 K, where the maximum reaction rates were used as intrinsic activity. The apparent activation energy for n-butane conversion on SZ-1 of 41.5 kJ/mol is in agreement with results reported previously [28,34,44].

Because SZ-2 showed no catalytic activity at 373 K for n-butane isomerization, we switched to He after 40 h and purged for 25 h; then we increased the temperature to 473 K and tested the catalytic performance again (see Fig. 8). Even though SZ-2 is almost inactive at 373 K, it showed activity for n-butane isomerization at 473 K, and the rate was on the same order as that of SZ-1 at 373 K. The selectivity for isobutane was 96–97% with SZ-2 at 473 K, and the major by-products were propane and pentane. SZ-2 deactivated only slowly.

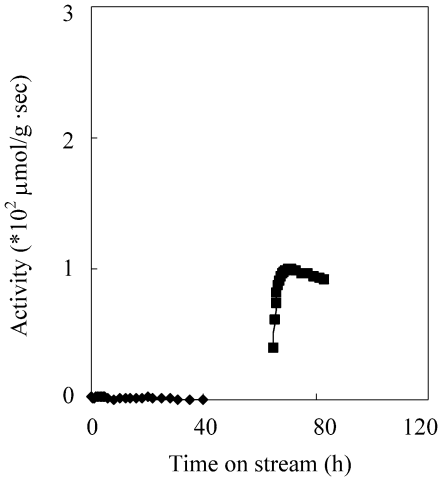

Fig. 8. *n*-Butane reaction rate on SZ-2 versus time on stream at (◆) 373 K followed by reaction at (■) 473 K.

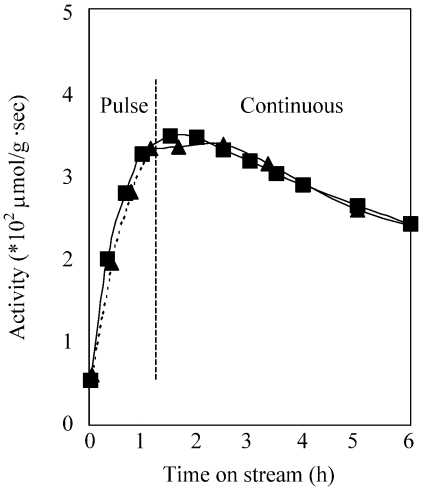

Fig. 9. *n*-Butane reaction rate on SZ-1 at 373 K (■) continuous reaction and (▲) pulse reaction during induction period (alternative pure helium and reactant per 1 min).

3.4.2. Pulsed reaction mode during the induction period

A pulse method was applied in this study to explore the catalytic behavior during the induction period. He and reactant were alternatively replaced every minute and passed into the reactor for the first 60 min during *n*-butane reaction at 373 K on SZ-1 (see Fig. 9). The overall reaction behavior was identical to the reaction with continuous flow, which indicates that the 1-min He purge did not affect the formation of active species. After the pulse reaction, a continuous flow of reactant was used to test the catalytic behavior in the deactivation period. It was also identical to the conventional continuous-flow reaction.

3.4.3. Stopping and restarting the reaction

We also investigated the stability of the active species on the catalytic surface by stopping and restarting the reaction during the deactivation phase. Fig. 10 shows that even after

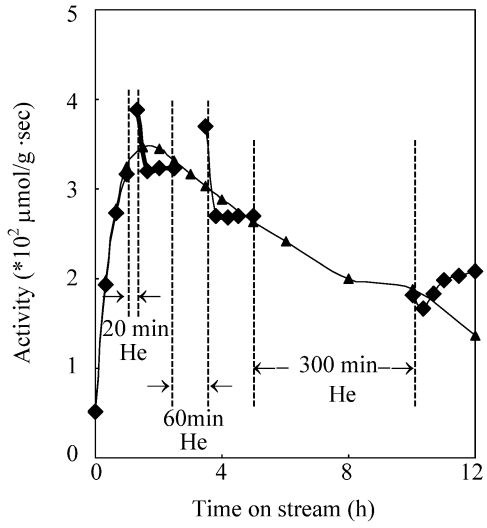

Fig. 10. *n*-Butane reaction rate on SZ-1 at 373 K (▲) continuous reaction and (◆) stop-restart reaction during deactivation period.

20, 60, 300 min of He purging, the catalyst showed high activity for *n*-butane isomerization without signs of a period of increasing activity. The average activity was nearly identical to that observed during the continuous-flow mode operation. It is obvious that the active species, the carbenium ion (alkoxy group), is stable at 373 K on the catalyst surface and is removed by He purge. However, the initial activity after the restart was always higher than that at steady state, indicating higher concentration of active species on the surface, which decreases to steady-state values after a short time.

3.5. TAP experiments on catalysts during continuous-flow operation

TAP experiments were conducted intermittently with flow experiments to investigate the adsorption and desorption during various stages of the life cycle of sulfated zirconia.

The TAP intensity profiles recorded at 423 K for fragment 43 (main fragment of *n*- and isobutane) are presented in Fig. 11. All measured data represent the overall response, which is determined by adsorption, desorption, and reaction [41]. As a single mass unit that can be used to follow the formation of products does not exist, fragmentation ratios are compared. Differences in the fragmentation patterns are thought to represent different surface processes and indicate indirectly the formation of products. Side product detection is also difficult because of the low intensities and the superposition of single mass fragments.

Relative to the inert materials corundum and unsulfated zirconia, the profile for the fresh SZ-1 was lower in intensity (not shown here). This consistently points to a strong interaction of *n*-butane and/or isobutane with SZ-1. The residence time (and hence the strength of interaction) increased in the presence of surface sulfates, as indicated by a com-

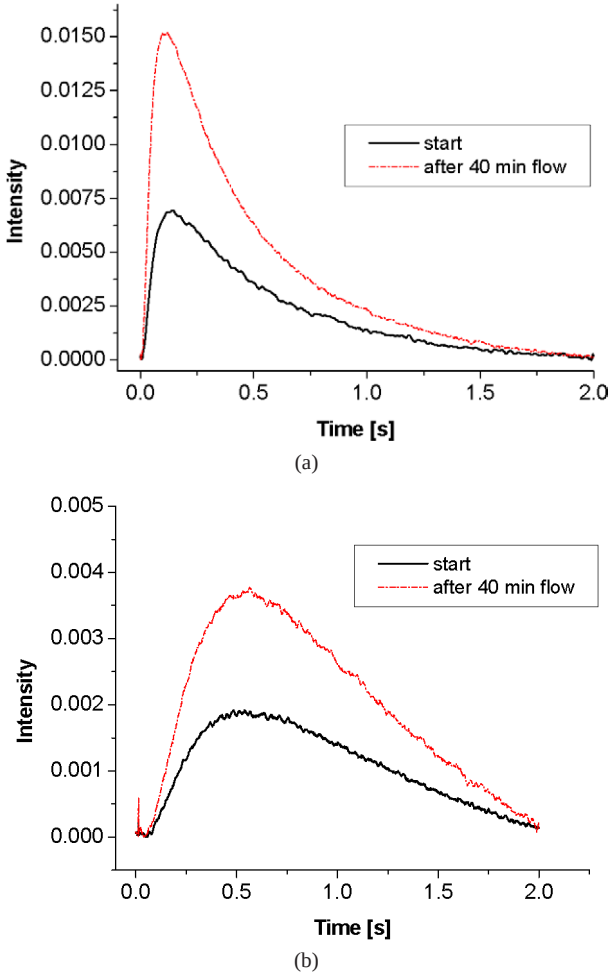

Fig. 11. TAP response pulses for n-butane ($m/e = 43$) at 423 K for two different reactivity states of the catalysts (a) SZ-1, (b) SZ-2.

parison of residence times between sulfated and nonsulfated samples.

After pulsing in vacuum, the operation mode was switched to flow conditions at atmospheric pressure for distinct time intervals. SZ-1 converted initially about 15% n-butane to isobutane and traces of propane and pentanes. With time on stream, SZ-1 deactivated to about 2% conversion after 120 min. After 40 min, the flow was stopped, and it was switched back to vacuum and n-butane pulses were admitted again. The residence times and fragmentation patterns discussed here are taken from pulsing after 40 min of treatment in n-butane flow, when SZ-1 is still active.

Table 2 summarizes all calculated fragmentation ratios. The comparison of the fragmentation ratios for SZ-1 (start values as a reference) and SZ-1 (40 min) clearly shows that, consistent with GC analysis, the conversion from n-butane to isobutane can be followed by changes in the main fragments 43, 27, 29, 41, and 58 here. All measured intensities vary in their intensity/fragmentation ratios. Because of possible irreversible adsorption on the surface during pulsing and flow, the mass balance is affected and may influence the measured ratios as well.

Table 2
Fragmentation pattern for SZ-1 and SZ-2 for fresh and deactivated catalysts (ratios of different mass fragments)

	43/20	58/20	43/58	27/20	29/20	41/20	42/20
SZ-1, fresh	1.73	0.18	9.31	1.82	1.96	0.33	0.43
SZ-1, 40 min	2.55	0.31	8.09	2.07	2.27	1.15	0.48
SZ-2, fresh	1.18	0.13	9.12	1.13	1.24	0.58	0.28
SZ-2, 40 min	1.40	0.15	9.20	1.39	1.43	0.69	0.29

Table 3
Comparison of residence times [s] for SZ-1 and SZ-2 for fresh and 40 min used catalysts ($m/e = 43$); over corundum $\tau = 0.08$ s, $T = 423$ K

	SZ-1	SZ-2
Fresh	0.52	0.84
40 min catalysis	0.46	0.83

In the TAP experiment, three trends were observed with increasing deactivation of SZ-1: (i) the intensity of the peaks slowly recovered compared with the inert material and increased (Fig. 11a), (ii) the residence times decreased, and (iii) the ratio of the m/e 43 to 58 fragments decreased (Table 3).

It is now interesting to compare the observed fragmentation ratios for SZ-2 with the same experimental setup. The measured response curves for SZ-2 (inactive under the conditions chosen) are shown in Fig. 11b. The displayed m/e 43 responses were reduced in their intensities relative to an inert material, too (inert material not shown). n-Butane is also strongly adsorbed to the surface of the material. The shape of the curves was broadened compared to SZ-1, and the residence time for the alkane was much higher than that observed for SZ-1. Evaluation of the online GC data revealed that no significant conversion of n-butane to isobutane was observed. This is also displayed by the constant fragmentation ratios of SZ-2 for the start reference values and the 40-min fragmentation pattern. With time on stream the intensity of the main fragments also increased, but their relations remained constant. Only adsorption and desorption determine the observed fragmentation ratios.

Modeling of the first step of the n-butane interaction with the catalyst surface was done with a simple one-zone model assuming first-order adsorption of the reactant. Comparison of the modeled adsorption rate constants for the fresh and used SZ-1 showed a significant decrease. As all parameters in the modeling are the same, the only variable that causes this decrease is the number of available adsorption sites on the catalyst surface. Thus it can be concluded that after 40 min of treatment of SZ-1 under flow conditions, nearly half of the available adsorption places are blocked or deactivated. It has to be noticed that in this simple model no term for reaction to the product is included. For SZ-2 the trend was opposite to that observed for SZ-1. After 40 min of treatment the adsorption rate constant was increased by a factor of 2.5, which can only be interpreted by assuming that adsorption site centers have been created.

4. Discussion

4.1. Prerequisites for active sites

It has been discussed for some time that an active sulfated zirconia catalyst must consist of the tetragonal phase, which is metastable below 1300 K. Only a few authors have claimed a monoclinic or a mixture of monoclinic and tetragonal sulfated zirconia to be active for *n*-butane isomerization [21,22]. In this study, however, two tetragonal sulfated zirconia samples prepared from zirconium hydroxides with different aging conditions exhibited very different catalytic activities for the *n*-butane reaction at low temperature. The tetragonal phase can thus be seen as a necessary but not sufficient requirement for good catalytic activity, which is consistent with the findings by Yang et al. [45].

Recent investigations by Li et al. [30] suggest that the isomerization reaction is initiated via oxidative dehydrogenation of *n*-butane by a pyrosulfate group ($S_2O_7^{2-}$). According to DFT calculations by Hofmann and Sauer [46], pyrosulfate is a possible and stable structure at the tetragonal (101) face. Following this hypothesis, two explanations emerge for the lower reactivity of SZ-2 in comparison with SZ-1, both based on the question of which circumstances will favor the formation of pyrosulfate.

SZ-1 and SZ-2 differ in the size of the crystalline domains (XRD), and, moreover, the short-range order (< 8 Å) of their structures is also decidedly different (Zr *K*-edge XAFS). Such variations in the bulk structure may lead to variations in the surface structure; more explicitly, the poorly crystallized, maybe highly defective tetragonal phase of SZ-2 may not be a suitable substrate for pyrosulfate. The pyrosulfate configuration on the zirconia surface is tetradentate; that is, the three oxygen atoms of the pyrosulfate are connected to three surface zirconium atoms, and a fourth oxygen is hydrogen-bridged to a water molecule adsorbed on a fourth zirconium atom. While the fourth link can be considered to be flexible, the other three bonds require three zirconium atoms arranged in an isosceles triangle. The lower intensity of the second shell in the EXAFS analysis of SZ-2 indicates that there are fewer zirconium atoms with the next zirconium neighbor at a distance corresponding to those of the tetragonal phase, implying that the described triangular configuration on the tetragonal (101) face is less abundant. The pyrosulfate, which is already strained on a perfect (101) face, may not be able to accommodate aberrations in the distances, whereas, for example, a bidentate monosulfate structure can.

The two samples SZ-1 and SZ-2 exhibit the same sulfate content, but different surface areas, resulting in different sulfate densities on the surface. The sulfate content is higher than required for a hypothetical monolayer coverage, that is, 5.2 and 7.2 wt% for SZ-1 and SZ-2, respectively, if we assume that the SO_4^{2-} group occupies an area of 0.31 nm^2 corresponding to its kinetic diameter [42]. However, the monolayer coverage depends on the assumed sulfate structure. In general, a higher sulfate density on the surface may lead to more condensed structures, such as pyrosulfates. Hence, more pyrosulfate configurations may exist on the surface of SZ-1 than on the surface of SZ-2, which would explain the higher activity of SZ-1.

The results confirm that highly active catalysts can be obtained with tetragonal materials; however, not all tetragonal materials are necessarily highly active. It is also required that the exposed facet planes be of the right type and right quality to allow the formation of certain sulfate structures. It is interesting in this respect that excellent promoters such as manganese or iron are incorporated into the tetragonal phase, causing a constriction of the lattice [47].

4.2. Dehydrogenation capacity of sulfated zirconia

The initial step of butane skeletal isomerization has been proposed to be the formation of a surface carbenium ion, but the mechanism of the formation of such an active species is still under debate. On a superacid catalyst, carbenium ions can be formed directly by the protonation of alkanes through Brønsted superacid sites and subsequent decomposition of the alkanium ions under cleavage of H_2 or by hydride abstraction from alkanes through Lewis superacid sites. However, the superacidity of sulfated zirconia has been in doubt recently, and the formation of carbenium ions was ascribed to the protonation of alkene impurities; the contribution of this pathway has been confirmed by the dramatic decrease in the isomerization activity after the removal of trace amounts of butenes in the feed.

In a preceding study, the dehydrogenation capacity of sulfated zirconia was identified during *n*-butane isomerization at 373 K by the detection of butene (with TPD), water (by in situ IR spectroscopy), and SO_2 [30]. The in situ generation of butenes has been shown to be the initial step for the *n*-butane isomerization reaction. Such a step would be noncatalytic if no pathways for reoxidation of the sulfur species existed and irreversible if sulfur were lost. However, once an activate intermediate has been formed, the isomerization proceeds in cycles, including rearrangement and hydride transfer with generation of new intermediates. Given a high number of cycles per generated butene, a pseudo-steady-state behavior can be observed.

The results for *n*-butane TPD on SZ-1 indicate that it is able to oxidatively convert *n*-butane to butene at low temperatures. However, for the catalyst SZ-2, which is inactive for *n*-butane isomerization at low temperatures, a discrete butene desorption peak was not observed. Thus we conclude that the dehydrogenation capacity of SZ-1, which leads to the in situ formation of butenes, is responsible for isomerization activity at low temperatures.

Increasing the reaction temperature to 473 K can effectively overcome the catalytic inactivity of SZ-2, which then shows an activity comparable to that of SZ-1 at 373 K. The activity is related to the oxidative dehydrogenation on SZ-2 at 473 K, either as less active sites become active or as

surface sulfate structures rearrange with temperature. In this context it should be emphasized that the heterogeneity of sulfated zirconia could lead to a wide spectrum of active sites with only a few very active ones being responsible for the reaction at low temperatures.

If the reaction is limited in the generation of alkenes, we conclude that at 373 K SZ-2 is not producing a sufficient quantity of butene to start the reaction. Thus, the difference in the generation of alkenes is responsible for the low activity of SZ-2. At 473 K the production of alkenes is sufficient for both materials, and, hence, catalytic activity is found on both. However, the rates of reaction still differ for the two materials by one order of magnitude (SZ-1, $r = 20 \times 10^{-2}$ μmol/(g s); SZ-2, $r = 1 \times 10^{-2}$ μmol/(g s)). In this context it should be emphasized that the concentration of Brønsted acid sites is 50% higher on SZ-1 than on SZ-2. This suggests that the dramatic differences between the two samples are the result of a number of subtle effects rather than one effect.

4.3. Adsorption sites and the nature of interaction with alkanes

The difference in catalytic activity between the two samples is not reflected in the number of sites available for alkane adsorption or in the differential heats. The projected coverage under our reaction conditions (5 kPa) for *n*-butane is 85–160 μmol g^{-1}. The sulfate content of both materials is 9 wt% or about 938 μmol g^{-1}. If a site consisted of a single sulfate group, only about 10–15% of all sulfate groups would participate under our reaction conditions; for a pyrosulfate group, about 20–30% of the sulfur would be involved in adsorption of the reactant. This confirms that not all sulfates are active and that the catalyst can be destroyed by the removal of 40% of the sulfate [48], and it may explain why it has been so difficult to identify any relevant sulfate structure spectroscopically.

The differential heats of adsorption for all three alkanes on the two catalysts did not deviate significantly from each other. Typically, about 60 kJ mol^{-1} evolved at low coverages, and beyond 10 μmol g^{-1} the heats dropped to 45–50 kJ mol^{-1}. These values correspond to only about 2–3 times the heat liberated upon condensation of propane (18.8 kJ mol^{-1}), *n*-butane (22.4 kJ mol^{-1}), and isobutane (21.3 kJ mol^{-1}) [49] and indicate a weak interaction.

The similarity of the heats of adsorption for C_3 and C_4 alkanes is explainable by an interaction with the surface that does not encompass the entire molecule. An adsorption with the *n*-alkane flat on the surface appears unlikely because of the corrugated nature of the sulfated zirconia surface [46]. The pocket-like interstitial space between the surface sulfate groups may accommodate only part of an alkane in an end-on-like fashion.

For the adsorption of *n*-alkanes on the zeolite HSZM-5, the heat of adsorption increases with the chain length; 32 and 48 kJ mol^{-1} were reported for the adsorption of propane and *n*-butane [50]. The range of 45–60 kJ mol^{-1} for the adsorption of propane and isobutane on sulfated zirconia indicates sites that interact more strongly with alkanes than those of the zeolite HZSM-5. Data for *n*-butane and isobutane adsorption on sulfated zirconia presented by González et al. [51] show a more rapid decline of the heat with coverage to values below 40 kJ mol^{-1} at 30 μmol g^{-1} coverage. The surfaces of SZ-1 and SZ-2 are obviously more homogeneous than those of the catalysts in [51].

Heats of adsorption from calorimetry data can be compared with those accessible through TAP data and can be used to validate the transferability of TAP results, which are obtained in the Knudsen regime (base pressure $< 10^{-9}$ hPa), to pressures in the hPa range. The heats of adsorption of *n*-butane that result from van't Hoff plots of the equilibrium constants given by the ratios of the rate constants for adsorption and desorption were similar for the two catalysts, namely, about 52–53 kJ mol^{-1}. The TAP response curve is an average over all interactions of the molecules in the pulse with the surface, and the obtained heat of adsorption should correspond to an average value. The average heat estimated from the calorimetric results is about 50 kJ mol^{-1}, indicating perfect agreement between the two techniques.

The heats of adsorption are relatively small, and adsorption at 313 K is reversible within the detection limits of the calorimeter (< 10%). The values obtained for the heats indicate a weak type of interaction for the majority of the alkane molecules, such as hydrogen bonding via induced polarization of the alkane. It has been reported that *n*-alkanes interact with the OH groups of pure [52] and sulfated zirconia [53]. The bands of sulfate were claimed not to be shifted appreciably after *n*-butane adsorption [54]; after adsorption of *n*-pentane the S=O band at 1416 cm^{-1} was decreased without the formation of additional bands. Thus the role of sulfate in the adsorption process is not clear, but it appears that alkanes adsorb on OH-groups.

Our results do not reveal an obvious difference in the quality of the sites for reactant adsorption that would allow an explanation of the order-of-magnitude difference in catalytic activities. The small heats of adsorption are consistent with the observations made during *n*-butane TPD, which did not show much desorption of butane because it is mostly weakly and thus reversibly adsorbed and is removed during evacuation before the TPD. However, the presence of a small number of sites with a different heat of adsorption cannot be excluded from calorimetry, and these might be the sites that dehydrogenate butane during TPD to give butene(s). The calorimetry results limit the number of sites capable of butane dehydrogenation to 5 μmol g^{-1} or less.

4.4. Carbenium ions and/or alkoxy groups on the surface at low temperature

An induction period was always observed during the *n*-butane isomerization reaction on sulfated zirconia at low

temperatures. It was concluded that during this period alkoxy groups (carbenium ions) formed by protonation of butene generated by oxidative conversion accumulated on the catalytic surface (see also Ref. [30]). On sulfated zirconia SZ-1, pulse and continuous-flow *n*-butane reaction at low temperature showed an identical induction period. The number of molecules streaming through the catalyst bed in the pulse experiment is only half of that in the continuous-flow experiment, indicating that the accumulation of a species by adsorption from the gas phase is not rate determining, as shown previously by Cheung et al. [55]. Rather, changes to the surface or slow conversion of already adsorbed species must be relevant. Furthermore, purging with helium did not affect the transition of the surface to a more active state. We speculate that some of the adsorbed *n*-butane molecules were retained on the surface because they have already been transformed and no longer interact merely by the weak interaction seen in the calorimetry and TAP experiments; that is, they could be surface carbenium ions.

The stop-restart method was applied in the deactivation period of *n*-butane isomerization. It is very clear that the active species are stable on the catalyst surface during He purge, even for 5 h. Thus, when the reaction was restarted, the reaction rate in the first minute is much higher compared with that of the continuous reaction, because a large fraction has been converted to *tert*-butyl carbenium ions, and these undergo preferred hydride transfer in this initial stage of the reaction. This is also why the catalytic activity, in the first minute after the reaction was restarted after 20 and 60 min of He purge, is higher than the maximum activity of the continuous-flow reaction. During He purge, the surface sec-butyl carbenium ion undergoes skeletal isomerization to its isomer, the tert-butyl carbenium ion, in the absence of *n*-butane. This suggests also that the skeletal isomerization and not the hydride transfer step is the rate-determining step. After the reaction was restarted following He purge for 5 h, the reaction showed an induction period, although the active species is still on the surface, indicating that the purge carried out over a long time can remove a very small fraction of the surface alkoxy groups/carbenium ions, probably via the decomposition of carbenium ion to its corresponding olefin and a proton.

In the deactivation period, without any butane flow, the deactivation rate of the stop-restart reaction was nearly identical to the continuous-flow reaction (at least for 20 and 60-min purges), which implies that the deactivation is due to the decay of the active species. The most plausible reaction is the reaction between olefins desorbing and surface carbenium ions forming larger surface intermediates, which hamper the accessibility to the active sites. The larger surface species also undergo slower hydride transfer. The rapid deactivation limits the use of bare sulfated zirconia in industry applications. Thus, usually a noble metal function is additionally introduced, and the reaction is carried out under hydrogen to control the olefin concentration in the reactor.

5. Conclusions

Two sulfated zirconia samples with different catalytic activities were fully characterized and investigated with respect to *n*-butane skeletal isomerization. The sulfated zirconia prepared from zirconium hydroxide aged in a solution at room temperature for 1 h showed much higher activity than that prepared from zirconium hydroxide aged at 373 K for 24 h. The stoichiometric oxidation (of butane to butene) of these two samples is concluded to be the critical difference determining the variations in catalytic activity. The SZ-2 sample exhibits catalytic activity when the reaction temperature is raised to 473 K, which indicates that the dehydrogenation property of sulfated zirconia was dramatically promoted by the higher temperature.

Since the two materials are tetragonal and have the same sulfate content, the difference in reactivity is speculated to originate from the difference in sulfate density on the surface (consequence of the BET surface areas), from the difference in the size and the defect structure of the zirconia crystals (revealed by XRD and EXAFS), or from a combination of these properties. The number of sites for butane oxidative dehydrogenation must be very small (less than 5 μmol/g), because microcalorimetry experiments prove the interaction with C_3 and C_4 alkanes to be weak for the majority of sites. Heats of adsorption for *n*-butane determined by calorimetry were about 45–60 kJ/mol, consistent with estimations from TAP data.

By analysis of the catalytic behavior of the surface active species, the surface alkoxy group/surface carbenium ion, with pulse and stop-restart methods on SZ-1 at 373 K, it was clearly shown that the carbenium ion is very stable under the conditions used, and the deactivation of sulfated zirconia is due to the decay of carbenium ion species.

Acknowledgments

The Deutsche Forschungsgemeinschaft is gratefully acknowledged for supporting this project in the framework of the priority program no. 1091, “Bridges between real and ideal systems in heterogeneous catalysis.” The authors thank E. Kitzelmann, R.E. Jentoft, T. Ressler, and the HASYLAB staff at DESY for the XAS and XRD measurements; G. Weinberg for the SEM measurements; and R. Schlögl, A. Hofmann, and J. Sauer for fruitful discussions. MEL Chemicals kindly provided the Y-stabilized ZrO_2.

References

[1] X.M. Song, A. Sayari, Catal. Rev. Sci. Eng. 38 (1996) 329.
[2] K. Arata, Adv. Catal. 37 (1990) 165.
[3] G.D. Yadav, J.J. Nair, Micropor. Mesopor. Mater. 33 (1999) 1.
[4] V. Adeeva, H. Liu, B. Xu, W.M.H. Sachtler, Top. Catal. 6 (1998) 61.
[5] T. Yamaguchi, K. Tanabe, Y.C. Kung, Mater. Chem. Phys. 16 (1986) 67.

[6] C. Sarzanini, G. Sacchero, F. Pinna, M. Signoretto, G. Cerrato, C. Morterra, J. Mater. Chem. 5 (1995) 481.
[7] C. Guo, S. Yao, J. Cao, Z. Qian, Appl. Catal. A Gen. 107 (1994) 229.
[8] J.R. Sohn, H.W. Kim, J. Mol. Catal. 52 (1989) 361.
[9] J.M. Parera, Catal. Today 15 (1992) 481.
[10] M.-T. Tran, N.S. Gnep, G. Szabo, M. Guisnet, Appl. Catal. A Gen. 171 (1998) 207.
[11] D. Fărcaşiu, J.Q. Li, Appl. Catal. A Gen. 175 (1998) 1.
[12] C. Morterra, G. Cerrato, C. Emanuel, V. Bolis, J. Catal. 142 (1993) 349.
[13] R.A. Comelli, C.R. Vera, J.M. Parera, J. Catal. 151 (1995) 96.
[14] A. Hahn, T. Ressler, R.E. Jentoft, F.C. Jentoft, Chem. Commun. (2001) 537.
[15] M. Hino, S. Kobayashi, K. Arata, J. Am. Chem. Soc. 101 (1979) 6439.
[16] C. Morterra, G. Cerrato, G. Meligrana, M. Signoretto, F. Pinna, G. Strukul, Catal. Lett. 73 (2001) 113.
[17] C.R. Vera, J.M. Parera, J. Catal. 165 (1997) 254.
[18] D. Fărcaşiu, J.Q. Li, S. Cameron, Appl. Catal. A Gen. 154 (1997) 173.
[19] D. Fărcaşiu, J.Q. Li, Appl. Catal. A Gen. 128 (1995) 97.
[20] F.R. Chen, G. Coudurier, J. Joly, J.C. Vedrine, J. Catal. 143 (1993) 616.
[21] W. Stichert, F. Schüth, J. Catal. 174 (1998) 242.
[22] W. Stichert, F. Schüth, S. Kuba, H. Knözinger, J. Catal. 198 (2001) 277.
[23] J.B. Nicholas, J.F. Haw, L.W. Beck, T.R. Krawietz, D.B. Ferguson, J. Am. Chem. Soc. 117 (1994) 12350.
[24] J. Zhang, J.B. Nicholas, J.F. Haw, Angew. Chem., Int. Ed. Engl. 39 (2000) 3302.
[25] B.S. Umansky, K. Hall, J. Catal. 124 (1990) 97.
[26] F. Babou, G. Coudurier, J.-C. Vedrine, J. Catal. 152 (1995) 341.
[27] L.M. Kustov, V.B. Kazansky, F. Figueras, D. Tichit, J. Catal. 150 (1994) 143.
[28] K.T. Wan, C.B. Khouw, M.E. Davis, J. Catal. 158 (1996) 311.
[29] D. Fărcaşiu, A. Ghenciu, J.Q. Li, J. Catal. 158 (1996) 116.
[30] X. Li, K. Nagaoka, L.J. Simon, A. Hofmann, J. Sauer, J.A. Lercher, J. Chem. Phys. B (2004), submitted for publication.
[31] J.E. Tabora, R.J. Davis, J. Am. Chem. Soc. 118 (1996) 12240.
[32] S. Hammache, J.G. Goodwin Jr., J. Catal. 211 (2002) 316.
[33] J.E. Tabora, R.J. Davis, J. Catal. 162 (1996) 125.
[34] A. Sayari, Y. Yang, X. Song, J. Catal. 167 (1997) 346.
[35] R. Ahmad, J. Melsheimer, F.C. Jentoft, R. Schlögl, J. Catal. 218 (2003) 365.
[36] K.B. Fogash, R.B. Larson, M.R. Gonzalez, J.M. Kobe, J.A. Dumesic, J. Catal. 163 (1996) 138.
[37] H. Liu, V. Adeeva, G.D. Lei, W.M.H. Sachtler, J. Mol. Catal. A 100 (1995) 35.
[38] P. Canton, R. Olindo, F. Pinna, G. Strukul, P. Riello, M. Meneghetti, G. Cerrato, C. Morterra, A. Benedetti, Chem. Mater. 13 (2001) 1634.
[39] T. Ressler, J. Synchrotron Rad. 5 (1998) 118.
[40] L.C. Josefowicz, H.G. Karge, E.N. Coker, J. Phys. Chem. 98 (1994) 8053.
[41] J.T. Gleaves, G.S. Yablonski, Y. Schuurman, Appl. Catal. A: Gen. 160 (1997) 55.
[42] N. Katada, J. Endo, K. Notsu, N. Yasunobu, N. Naito, M. Niwa, J. Phys. Chem. B 104 (2000) 10321.
[43] S. Matysik, C. Breitkopf, H. Papp, submitted.
[44] C.-Y. Hsu, C.R. Heimbuch, C.T. Armes, B.C. Gates, J. Chem. Soc. Chem. Commun. 1645 (1992).
[45] X. Yang, R.E. Jentoft, F.C. Jentoft, Catal. Lett., in press.
[46] A. Hofmann, J. Sauer, J. Phys. Chem. B 108 (2004) 14652.
[47] F.C. Jentoft, A. Hahn, J. Kröhnert, G. Lorenz, R.E. Jentoft, T. Ressler, U. Wild, R. Schlögl, J. Catal. 224 (2004) 124.
[48] X. Li, K. Nagaoka, J.A. Lercher, J. Catal. (2004), in press.
[49] D'Ans Lax, Taschenbuch für Chemiker und Physiker (Handbook for Chemists and Physicists), Organic Compounds, vol. II, fourth ed., Springer, Berlin, 1983.
[50] F. Eder, M. Stockenhuber, J.A. Lercher, J. Phys. Chem. B 101 (1997) 5414.
[51] M.R. González, K.B. Fogash, J.M. Kobe, J.A. Dumesic, Catal. Today 33 (1997) 303.
[52] B. Klose, Thesis (Diplomarbeit), TU München 2001.
[53] E.A. Paukshtis, N.S. Kotsarenko, V.P. Shmachkova, Catal. Lett. 69 (2000) 189.
[54] F. Babou, G. Coudurier, J.C. Vedrine, J. Catal. 152 (1995) 341.
[55] T.-K. Cheung, J.L. d'Itri, B.C. Gates, J. Catal. 151 (1995) 464.